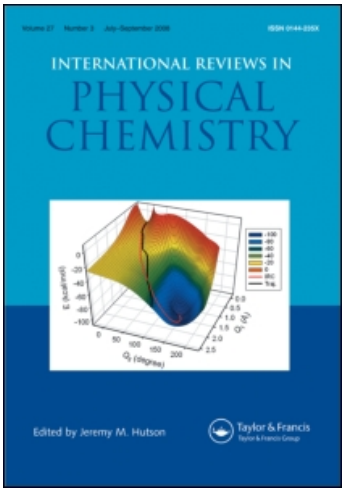

International Reviews in Physical Chemistry
Publication details, including instructions for authors and subscription information:
http://www.informaworld.com/smpp/title~content=t713724383

Probing solution-phase species and chemistry in the gas phase

Xue-Bin Wang; Xin Yang; Lai-Sheng Wang

Online publication date: 26 November 2010

To cite this Article Wang, Xue-Bin , Yang, Xin and Wang, Lai-Sheng(2002) 'Probing solution-phase species and chemistry in the gas phase', International Reviews in Physical Chemistry, 21: 3, 473 — 498
To link to this Article: DOI: 10.1080/01442350210157348
URL: http://dx.doi.org/10.1080/01442350210157348

INT. REVIEWS IN PHYSICAL CHEMISTRY, 2002
VOL. 21, NO. 3, 473–498

Probing solution-phase species and chemistry in the gas phase

XUE-BIN WANG, XIN YANG and LAI-SHENG WANG

Department of Physics, Washington State University, 2710 University Drive, Richland, WA 99352, USA, and W. R. Wiley Environmental Molecular Sciences Laboratory, MS K8-88, PO Box 999, Pacific Northwest National Laboratory, Richland, WA 99352, USA

Electrospray ionization not only is a powerful soft ionization technique for biological mass spectrometry but also provides an unique interface between the solution phase and the gas phase. An experimental apparatus combining electrospray with photodetachment photoelectron spectroscopy has been developed for the investigation of multiply charged anions and solution-phase species in the gas phase. In this article, the principles of this technique and our recent progress are presented and discussed. Photoelectron spectroscopy is ideal to probe free multiply charged anions and has allowed the repulsive Coulomb barrier existing universally in multiply charged anions to be directly observed and investigated. Solvation effects, solvent and counter-ion stabilization of a common inorganic doubly charged anion, SO_4^{2-}, have been extensively investigated. The minimum number of water molecules needed to stabilize SO_4^{2-} and its solvation behaviour have been addressed. Large hydrated SO_4^{2-} clusters are found to exhibit properties of bulk aqueous solutions. We also show that the electronic structures of many inorganic metal complexes, in particular redox species, can be investigated in the gas phase using electrospray and photoelectron spectroscopy.

Contents

International Reviews in Physical Chemistry ISSN 0144–235X print/ISSN 1366–591X online © 2002 Taylor & Francis Ltd
http://www.tandf.co.uk/journals
DOI: 10.1080/01442350210157348

1. Introduction

Many important chemical reactions including all biologically related processes take place in aqueous solution. Understanding the properties of aqueous electrolyte solutions at a molecular level has been the focus of intensive research recently [1–6]. However, the complications of the bulk environments present considerable challenges for obtaining a molecular-level understanding of phenomena in solution phase. Gas-phase solvated clusters have been used as models to obtain insight into the solution phase, and many gas-phase techniques as well as theoretical methods have been developed to investigate solvated species [7–25]. Most of the current research efforts on solvated ions have been devoted to the simple atomic cations or anions [15–20] with few efforts on more complex ions, in particular complex anions [21–24]. The use of atomic ions simplifies the spectroscopy and dynamics of the solvated clusters and allows better experimental controls. For example, dynamic processes, such as the 'cage' effect and cluster relaxation, have been revealed using ultrafast spectroscopy on simple solvated iodide anions [24, 25].

Multiply charged anions (MCAs) are ubiquitous in the condensed phase and constitute an important class of complex anions. However, free MCAs have been difficult to study and very few of them were known in the gas phase previously [26–33]. This is partly due to the fact that many MCAs acquire their stability in the condensed phase through solvation and other electrostatic interactions and are not stable in the gas phase and partly due to the lack of a generic method for producing MCAs in the gas phase. Studies of free MCAs are interesting for several reasons. First, MCAs are dominated by their intramolecular Coulomb repulsions arising from the excess charges, which make many MCAs unstable as isolated species. Gas-phase studies provide a rare opportunity to examine the intramolecular Coulomb repulsion and the intrinsic stabilities of MCAs. Second, many inorganic metal complexes and redox species exist in solution as MCAs. It would be highly desirable to probe their intrinsic molecular properties without the complication of the condensed phase environments. The obtained molecular and spectroscopic information can be used to compare directly with theoretical calculations, which are often done on gaseous species. Third, it is of fundamental chemical and physical significance to understand how an unstable MCA can be stabilized in the gas phase by solvent or counterions. Such investigations also provide an excellent opportunity to probe the solute–solvent interactions for a class of important complex anions. Furthermore, solvated clusters of complex anions may be used as structural models and molecular analogues for the investigation of the physical and chemical properties of electrolyte solutions in the gas phase.

During the past few years, we have developed an experimental technique combining electrospray ionization (ESI) and photodetachment photoelectron

spectroscopy (PES) that allows us not only to probe free MCAs but also to access a wide variety of solution-phase anions in the gas phase [33, 34]. ESI is a powerful soft-ionization method for biomolecules [35]; it is also an ideal technique to produce MCAs, as well as any ionic species and solvated clusters from solutions to the gas phase [36–39]. PES provides a powerful experimental technique to probe the electronic structure and intrinsic stabilities of MCAs in the gas phase [33]. It directly measures the excess electron binding energies in MCAs, thus allowing information about their stabilities and intramolecular Coulomb repulsions to be obtained straightforwardly. The combination of ESI and PES also provides a general and sensitive tool to probe solution-phase species and solvated clusters of both simple and complex anions in the gas phase.

Some of our initial findings using PES to probe free MCAs, such as the observation of the repulsive Coulomb barrier (RCB), the relationship between the RCB and the intramolecular Coulomb repulsion, and the first experimental observation of a negative electron binding energy in a molecule, were reviewed in 2000 [33]. In the current article, we summarize our recent progress in understanding free MCAs since then. In particular, we review our new research effort on probing a variety of solution-phase species in the gas phase, including the subject of solvation and solvent stabilization of complex MCAs and stabilization of MCAs by counter-ions. We also present studies of the electronic structures of many metal complexes in the gas phase. We show especially how intrinsic properties of redox species and redox reactions can be probed in the gas phase using PES.

This article is organized as follows. In the next section, the experimental apparatus and principles are described. After a brief overview of the advances in understanding MCAs, we present in section 3 our recent efforts with free MCAs, i.e. the observation of anisotropy of the RCB, the origins of stabilities of two similar small dicarboxylate dianions and a very high second electron binding energy in ZrF_6^{2-}. The solvation effect, solvent and counterion stabilization of unstable gaseous MCAs are presented in section 4. The uniqueness of solvation of MCAs and the direct observation of transition from gas-phase clusters to nano-droplets that show properties of bulk aqueous solutions are presented. Details of the electronic structures of metal complexes, as well as information about the intrinsic reorganization energies of redox species, are summarized in section 5. Finally some concluding remarks are given in section 6.

2. Experimental methods

The apparatus that we have developed couples an ESI source and ion-trap mass spectrometry with a magnetic-bottle time-of-flight (TOF) photoelectron spectrometer [34]. The limitation of ESI is that the anions of interest have to be present in the original solution. The advantage is that it is a soft ionization tool that simply transports the solution phase species into the gas phase. For MCAs, ESI avoids the sequential electron attachment processes that would be required if they are to be formed from neutral molecules. ESI is generally applicable to a wide range of MCAs as long as they exist in solution and are long lived in the gas phase. The electronic stability of an MCA can be determined directly from the threshold feature of its PES spectrum. The features in a PES spectrum of an MCA represent transitions from the electronic ground state of the MCA to the ground and excited states of the corresponding final species with one electron removed. Using the single-particle

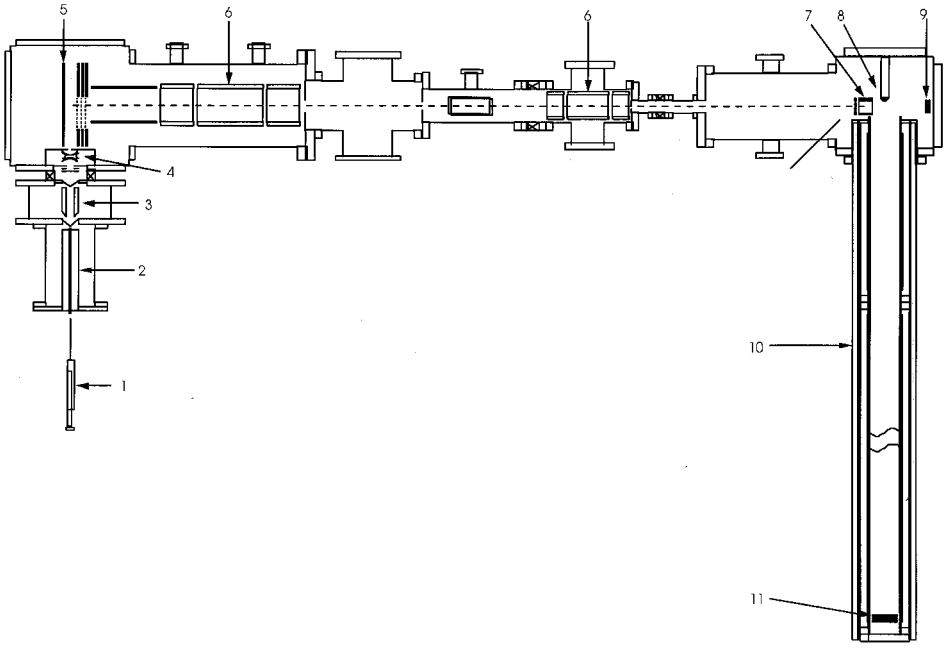

Figure 1. Schematic view of the electrospray–photodetachment apparatus: 1, syringe; 2, heated desolvation capillary; 3, radio-frequency quadrupole ion guide; 4, quadrupole ion trap; 5, TOF mass spectrometer extraction stack; 6, Einzel lens assembly; 7, three-grid mass gate and momentum decelerator assembly; 8, permanent magnet (NdFeB); 9, 40 mm dual microchannel plate in-line ion detector; 10, 4 m TOF tube with a low-field solenoid and double-layer μ-metal shielding; 11, 18 mm Z-stack microchannel plates photoelectron detector. From [34].

picture (Koopmans' theorem), these PES features can be alternatively viewed as removing electrons from the occupied molecular orbitals of the initial anions. Therefore, PES also provides direct information about the electronic structure and chemical bonding of the MCAs.

Details of our apparatus were described elsewhere [34]. Figure 1 gives a schematic overview. The critical components of this apparatus are the ion trap and the magnetic-bottle PES analyser. ESI, being intrinsically continuous, is not compatible with TOF analysis at low repetition rates. The use of the ion trap allows ions to be accumulated, greatly enhancing the sensitivity of the TOF mass analysis. The magnetic-bottle PES analyser, although intrinsically an angle-integrated technique, has the highest sensitivity for photoelectron analysis.

We usually use a water:methanol (30:70 ratio) mixed solution or a pure acetonitrile solution containing the anions of interest and spray it at ambient conditions using a syringe (1), whose tip is biased at a negative high voltage through a stainless steel tubing. The highly charged liquid droplets produced are fed into a desolvation capillary (2), which is heated to ~50–100°C. The anions that emerge from the desolvation capillary are guided by an RF-only quadupole system (3) into a quadrupole ion trap (4). The anions are usually accumulated for about 0.1 s before being pushed out into a TOF mass spectrometer (5, 6, 9) for mass and charge analyses. The desired anions are selected by a mass gate (7) and decelerated before

being detached by a laser beam in the interaction zone of the magnetic-bottle PES analyser (8, 10, 11). Several detachment photon wavelengths are used, ranging from 532 nm (2.331 eV), 355 nm (3.496 eV) and 266 nm (4.661 eV) with an Nd:YAG laser to 193 nm (6.424 eV) and 157 nm (7.866 eV) with an excimer laser. The photoemitted electrons are collected at nearly 100% efficiency by the magnetic bottle and analysed by the 4 m long electron flight tube (10). The ion trap and TOF mass spectrometer are operated at 10 Hz repetition rate while the magnetic-bottle PES analyser is operated at 20 Hz with the ion beam off during alternating laser shots for background subtraction, which is necessary at 266, 193 and 157 nm detachment wavelengths. The photoelectron kinetic energies are usually calibrated with the known spectra of O^- and I^-. The resolution of the magnetic-bottle PES analyser is about 2% ($\Delta KE/KE$), i.e. ~10 meV for 0.5 eV electrons.

3. Probing free MCAs in the gas phase using photoelectron spectroscopy

3.1. *Brief overview of recent advances in studies of free MCAs*

MCAs are commonly found in solutions and solids. Their stability outside the condensed phases is dominated by the Coulomb repulsion between the excess charges. Free MCAs are interesting gaseous species that provide opportunities to understand intramolecular electrostatic interactions and solvation effects. Several early reviews are available on gas-phase observations of MCAs [26–31]. More comprehensive reviews are given in our feature article [33] as well as more recently by Dreuw and Cederbaum [32].

The most significant recent advances in experimental studies of MCAs have been the PES investigations from our group. We have studied a number of free MCAs, including organic dianions [40–42], doubly charged inorganic metal complexes [43–45] and a quadruply charged anion, copper phthalocyanine tetrasulphonate tetraanion [46, 47]. The smallest dianions that we were able to observe are the pentaatomic species PtX_4^{2-} and PdX_4^{2-} (X = Cl, Br), which in fact were shown to be metastable [45] against loss of an X^- ligand. $PtCl_4^{2-}$ and $PtBr_4^{2-}$ were also found to be metastable against loss of an electron. We directly observed the existence of the RCB against electron detachment in MCAs and were able to estimate its magnitude using photon-energy-dependent studies [40, 41]. The RCB, universally present in MCAs against electron detachment or charge separation fragmentation, is created as a result of the superposition of the short-range binding of the excess electrons and the long-range Coulomb repulsion between two negatively charged particles, as schematically shown in figure 2 for electron emission. We found profound effects of the RCB on photodetachment processes and the resulting PES spectra. In particular, we observed that no photoelectrons can be measured even when a photon energy is above the binding energy of a given detachment channel, if the photon energy is below the corresponding RCB. This has become a universal signature of PES of MCAs, rendering threshold photodetachment infeasible. More importantly, we found that the RCB is equal in magnitude to the Coulomb repulsion between the excess charges at the equilibrium structure of an MCA [41]. The RCB provides dynamic stability and even traps the unbound excess electrons in MCAs (figure 2(*b*)). In fact, we have directly observed negative electron binding energies in the copper phthalocyanine tetrasulphonate tetraanion [46, 47] and in $PtCl_4^{2-}$ and $PtBr_4^{2-}$ [45], where the RCB provides substantial lifetimes for these metastable MCAs. We have also observed electron-tunnelling effects through the RCB and interpreted the

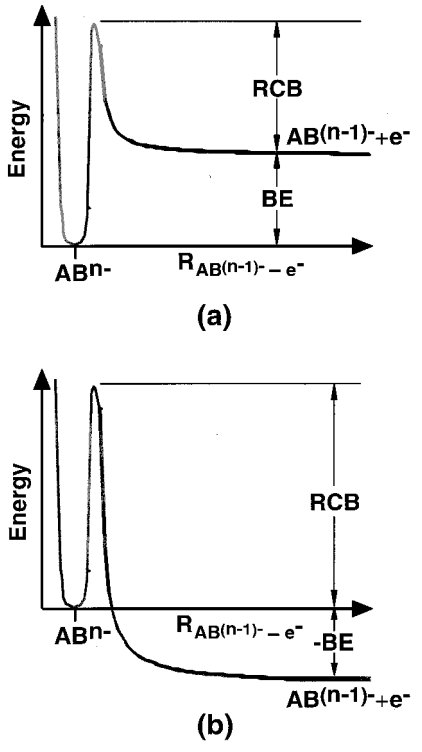

Figure 2. Schematic potential energy curves showing the excess electron binding energy (BE) and the RCB in MCAs: (*a*) for an electronically stable MCA with a positive BE; (*b*) for an electronically unstable MCA with a negative BE.

tunnelling data using a model Coulomb potential developed for α decay in nuclear physics [45, 48]. These initial findings have been recently reviewed in depth [33]. In sections 3.2 and 3.3, we present some of our new observations about MCAs since then.

3.2. *Intramolecular Coulomb repulsion and anisotropies of the RCB in MCAs*

We have devised a simple, schematic one-dimensional potential curve to understand and represent the RCB in MCAs and its effects on the PES spectra (figure 2) [40–48]. In reality, except for atomic species or completely spherical molecules, the RCB is expected to be complicated, multidimensional and anisotropic [49]. The one-dimensional RCB model may be considered to be along the direction of minimal Coulomb repulsion for electron detachment. In principle, the anisotropy of the RCB can be measured using angle-resolved PES, which is not feasible in our current apparatus since the magnetic-bottle PES analyser, necessary to enhance the collecting efficiency, is an angle-integrated technique. Dreuw and Cederbaum have recently calculated the RCB for a linear dianion, $[C{-}C{-}Be{-}C{-}C]^{2-}$ [49], and they indeed found a strong anisotropy in removing an electron from the highest-occupied molecular orbital of the linear BeC_4^{2-} dianion depending on the angle of emission relative to the molecular axis. The highest barrier was observed to be along the direction of the molecular axis and the lowest barrier is along the C_2 axis

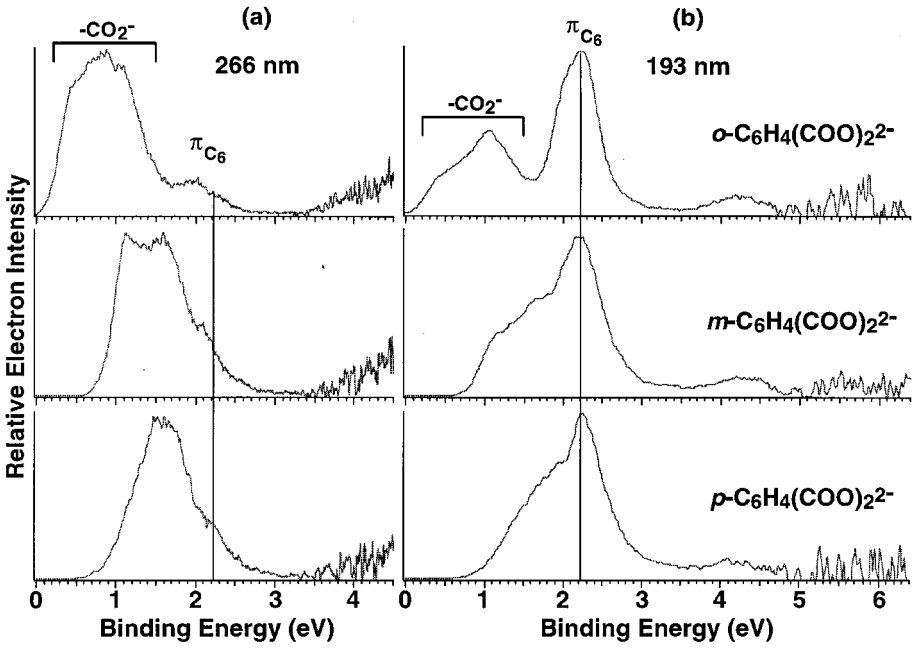

Figure 3. Comparison of the (*a*) 266 and (*b*) 193 nm spectra of the three benzene dicarboxylate dianions, showing the similar binding energies of the 2.2 eV feature due to the ring π electrons (π_{C6}) in the three isomers and their change at 266 nm due to the RCB. The threshold features due to detaching electrons from the charge carriers, $^{-}CO_2^{-}$, vary in the three isomers owing to the different charge separations. From [50].

perpendicular to the molecule, which can be easily understood from the charge distributions of the dianion.

In principle, a different RCB anisotropy can arise depending on which molecular orbital an electron is removed from. It can be conceived that different spatial distributions of different molecular orbitals can give rise to different RCBs for electron detachment. We have indeed observed such an anisotropy or inequivalence of RCBs for different detachment channels within the same MCA from the PES spectra of the three isomers of the benzene dicarboxylate dianion (BDC^{2-}) [50]. The photoelectron spectra of *o*-, *m*- and *p*-BDC^{2-} are shown in figure 3 at two detachment photon wavelengths, 266 and 193 nm. For all three dianions, rather congested spectra were obtained. The PES spectra of *o*-BDC^{2-} show two characteristic groups of features, as seen more clearly in the 193 nm spectrum. The first group at lower binding energies consists of features between the threshold and about 1.6 eV. There are probably several unresolved electronic transitions in this spectral range. The second group, consisting of a broad band, is centred around 2.2 eV. Interestingly, the 2.2 eV feature seems to be present in the spectra of all three dianions with nearly identical binding energies, as indicated by the full line in figure 3. It appears that the first group of features is also present in the spectra of *m*- and *p*-BDC^{2-}, although they are shifted to higher binding energies, resulting in the seemingly more congested spectra in the latter cases. The first group of features is from detachment of electrons of the carboxylate groups (CO_2^{-}) and the second group to be from the π system of the ring (π_{C6}). This assignment is reasonable, considering

the fact that there is less Coulomb repulsion between the two carboxylates in *m*- and *p*-BDC^{2-} and the electron binding energies related to the carboxylates are expected to increase relative to *o*-BDC^{2-}. On the other hand, the Coulomb repulsion between the two negative charges (mainly localized on the carboxylates) and the π electrons of the ring is expected to be similar in the three isomers. Thus, it is understandable that the binding energies of the ring π electrons would be similar in all three dianions.

The intensity of the ring π electron features decreases significantly in the 266 nm spectrum (figure 3(*a*)). This observation suggests that the energy of the 266 nm photon is lower than the RCB for the detachment channel of the ring π system (designated as RCB(π_{C6})), whereas the energy of the 193 nm photon is above RCB(π_{C6}) for all three isomers. The RCB(π_{C6}) for all three isomers was thus estimated approximately to have the same magnitude: $2.5\,\text{eV} < \text{RCB}(\pi_{C6}) < 4.2\,\text{eV}$. On the other hand, the RCB for detachment from the carboxylate groups (RCB(CO_2^-)) was estimated from the photon-energy-dependent PES spectra to be ~3.0, ~2.3 and ~1.9 eV for the *o*-, *m*- and *p*-BDC^{2-} respectively. The trend of RCB(CO_2^-) is consistent with that of the intramolecular Coulomb repulsion between the two carboxylate groups. Therefore, we found that the RCBs for detaching electrons from the carboxylate or from the ring π orbitals are quite different for each BDC^{2-} dianion. This anisotropy of the RCB is related to the different locations of the removed electrons within the same MCA. For relatively large MCAs, this anisotropy is expected to be common and the RCB cannot be assumed to be the same for all detachment channels for a given MCA.

3.3. *Stabilities of two small dicarboxylate dianions: acetylene dicarboxylate and succinate*

The stability of an MCA is mainly determined by the intramolecular Coulomb repulsion, i.e. the size of the molecule. However, there are other electronic and structural factors important to the stability of a given MCA. For example, despite their similar charge separation and size, $(O_2C–C{\equiv}C–CO_2)^{2-}$ (AD^{2-}) and $(O_2C–CH_2CH_2–CO_2)^{2-}$ (SD^{2-}) appear to have very different electronic stabilities, because AD^{2-} was observed abundantly, whereas SD^{2-} was very difficult to detect [51]. The PES spectra of the AD^{2-} dianion were obtained at 355, 266 and 193 nm (figure 4) with 0.30 ± 0.10 and 0.60 ± 0.10 eV adiabatic and vertical electron binding energies respectively. *Ab initio* calculation carried out by Skurski and Simons predicted that AD^{2-} is adiabatically stable with respect to electron loss whereas SD^{2-} is not [51] consistent with our experimental observations. The calculations showed that AD^{2-} has a D_{2d} structure with 0.42 and 0.69 eV adiabatic and vertical electron binding energies, respectively, which compared well with the corresponding experimental values. SD^{2-} was found to have a C_{2h} structure with a negative adiabatic electron binding energy (−0.086 eV), which explained the difficulty of observing SD^{2-} from our ESI source. Detailed theoretical analysis indicated that while the two excess charges in SD^{2-} are completely localized on the terminal carboxylate groups, there is significant delocalization of the excess charges into the –CC– π-type orbitals in AD^{2-}. The D_{2d} structure of the AD^{2-} dianion allows each carboxylate to interact with one of the two perpendicular π-type orbitals of the acetylene moiety, thus providing extra stabilization while minimizing the Coulomb repulsion.

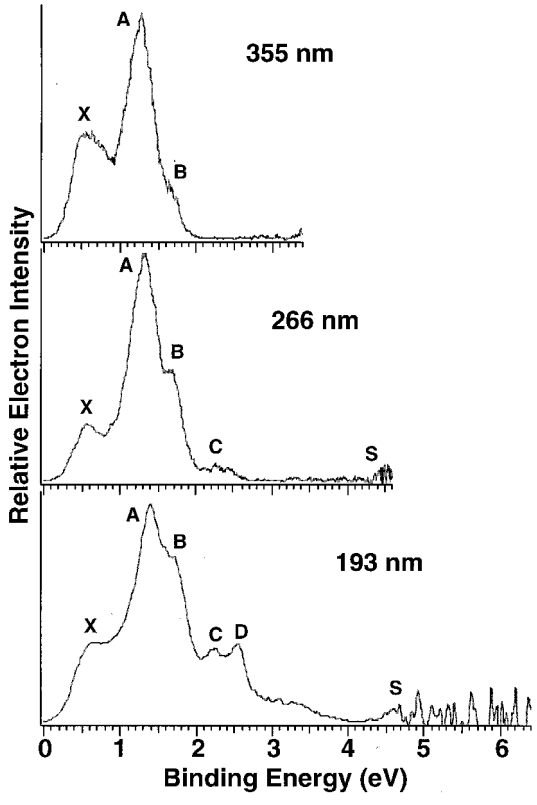

Figure 4. Photoelectron spectra of $(O_2C–C{\equiv}C–CO_2)^{2-}$ at three photon energies. From [51].

3.4. *Observation of a very high second electron affinity*

Electron affinity (EA) is an important molecular property of a molecule. Molecules with high EAs are strong oxidizing agents and form extremely stable anions. The first-order EAs of many atomic and molecular species have been measured [52]. However, despite much early theoretical work [53–56], very little is known experimentally about the second- or higher-order EAs for any molecular species [57] until very recently with the development of our ESI–PES apparatus. To determine the second- or higher-order EAs, MCAs are involved. Because of the RCB, PES provides an ideal technique to measure higher-order EAs. The adiabatic detachment energy (ADE) of the ground state transition in a PES spectrum of any MCA represents a higher-order EA. An example of a very high second-order EA was found in the PES spectra of ZrF_6^{2-}, for which a very high second EA was theoretically predicted [58, 59].

We obtained the PES spectra of the ZrF_6^{2-} at both 193 and 157 nm [60], as shown in figure 5. The spectra revealed three features, corresponding to detaching electrons from the top three occupied molecular orbitals of the ground state of ZrF_6^{2-}. We measured a vertical detachment energy of 3.4 eV for the ground-state transition, confirming the high detachment energy predicted for ZrF_6^{2-}. We found actually that the theory has substantially overestimated the detachment energy. The broad width of the ground-state transition may also suggest that the singly charged ZrF_6^- species is unstable against dissociation, owing to the relatively weak Zr–F chemical bonding.

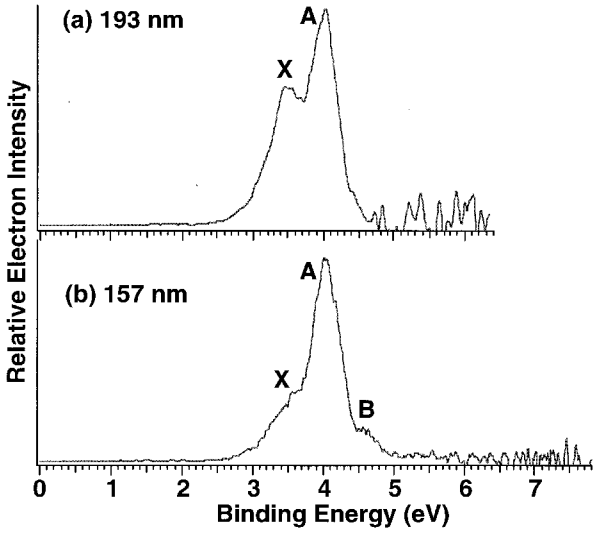

Figure 5. Photoelectron spectra of ZrF_6^{2-} at two photon energies. From [60].

In fact, we found that, although the second electron is strongly bonded in ZrF_6^{2-}, this dianion is metastable relative to loss of an F^- owing to the strong Coulomb repulsion and the relatively weak Zr–F bond. We were also able to estimate the lifetime of ZrF_6^{2-} using our ion trap and obtained a decay half-life of about 4 s [60], confirming its thermodynamic metastability, as also predicted theoretically [58, 59].

4. Stabilization of MCAs in the gas phase: from solvated clusters to nano-droplets

Many familiar inorganic MCAs are not stable as isolated species because of the strong intramolecular Coulomb repulsion among the excess charges, whereas they are stabilized in the condensed phase by solvation in solution or counterions in solid. It would be of fundamental chemical and physical significance to understand how MCAs are stabilized in the gas phase by solvent or counterions. Such investigations provide molecular-level information about the solvation of a complex MCA, as well as helping us to understand its properties in electrolyte solutions, on surfaces and at interfaces. Hydration of several common inorganic MCAs has been investigated both experimentally [36] and theoretically [61]. The counterion stabilization of C_9^{2-} by Cs^+ has also been examined both theoretically and experimentally [62, 63].

4.1. *Counterion stabilization of SO_4^{2-}*

SO_4^{2-} is a very common inorganic anion in the condensed phase. However, isolated SO_4^{2-} was found to be unstable to autodetachment in the gas phase [64–66]. One strategy to stabilize it was through attachment of a counterion, forming an ion pair. The counterion only interacts with the dianion electrostatically, allowing the electronic structure of an isolated SO_4^{2-} to be experimentally accessed. Such ion pairs may also be present in concentrated aqueous solutions.

We were able to observe abundant alkali metal sulphate ion pairs and their doubly charged dimers in the gas phase, i.e. $Na^+SO_4^{2-}$, $K^+SO_4^{2-}$, $(NaSO_4)_2^{2-}$, $(KSO_4)_2^{2-}$ and $[NaK(SO_4)_2]^{2-}$, using ESI and measured their PES spectra [67]. Figure 6 presents the spectra of $NaSO_4^-$ and KSO_4^- measured at three photon

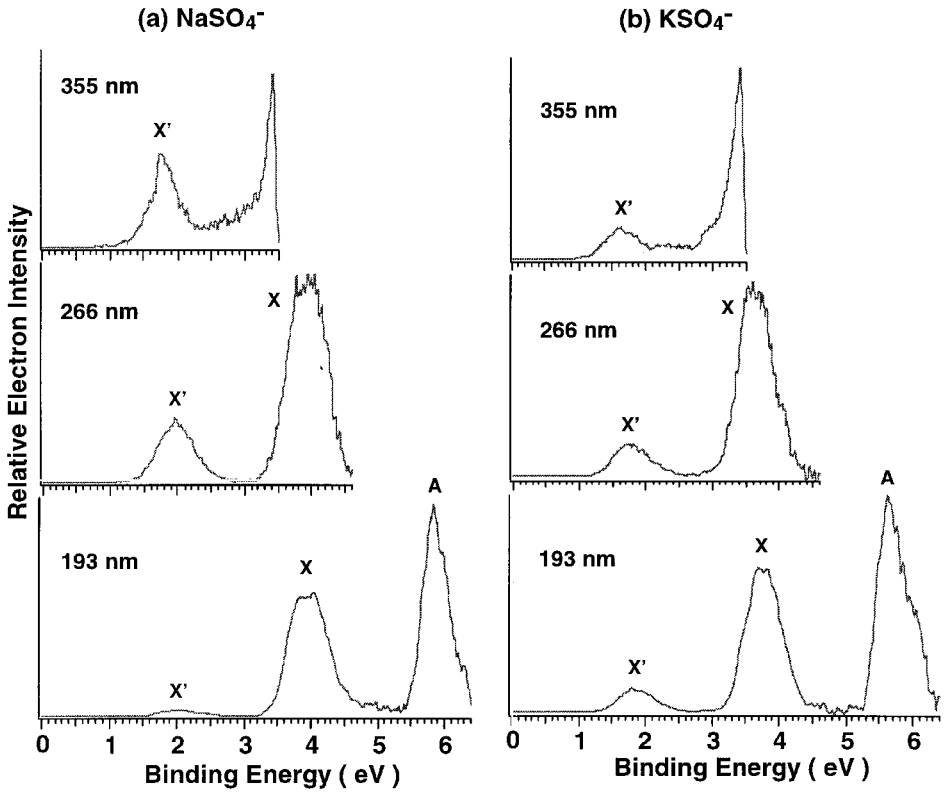

Figure 6. Photoelectron spectra of (*a*) $NaSO_4^-$ and (*b*) KSO_4^- at 193, 266 and 355 nm. Note the X′ peaks at 355 nm are shifted to a lower binding energy by 0.2 eV compared with those of the 266 and 193 nm spectra. The X′ peaks are due to the $[NaSO_4]_2^{2-}$ and $[KSO_4]_2^{2-}$ dimer dianions. From [67].

energies. Very similar spectral features were observed for KSO_4^- and $NaSO_4^-$, except that the binding energies of KSO_4^- are slightly lower. The 193 nm spectra show three well-separated and rather broad features, labeled X', X, and A. The intensity of the X' feature is unusually low and changes with the ESI source conditions and was due to the dimer dianion $[MSO_4]_2^{2-}$ (M = Na, K).

In order to confirm the existence of the doubly charged dimer anions, we sprayed a mixed solution of Na_2SO_4 and K_2SO_4, intending to produce $NaK(SO_4)_2^{2-}$, which has an m/z value of 127, different from both $NaSO_4^-$ ($m/z = 119$) and KSO_4^- ($m/z = 135$). The mixed dianion was indeed observed. The PES spectra of $NaK(SO_4)_2^{2-}$ are shown in figure 7 at 355, 266 and 193 nm. The sharp peaks in figure 7 are due to I^-, which has an identical m/z ratio to $NaK(SO_4)_2^{2-}$. I^- was present as an impurity because we used it daily to calibrate our spectrometer and could not completely eliminate it from our system. Nevertheless, two PES features (X' and A') were clearly observed in the 193 nm spectrum of $NaK(SO_4)_2^{2-}$, one starting at 1.5 eV (X') and one starting at 3.6 eV (A'). The latter is overlapped with one of the transitions from I^-. As expected, the X' feature from the spectra of $NaK(SO_4)_2^{2-}$ is almost identical to that observed in the spectra of $NaSO_4^-$ and KSO_4^- and showed a similar spectral shift at 355 nm. Furthermore, the A'

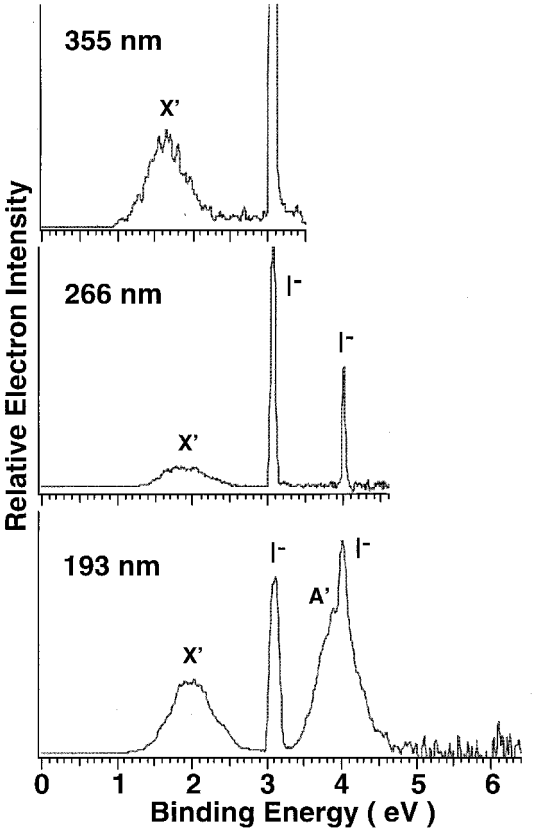

Figure 7. Photoelectron spectra of $[NaK(SO_4)_2]^{2-}$ $(m/z = 127)$ at three photon energies. The two sharp peaks are from I^- $(m/z = 127)$ contamination. Note that the doubly charged anions have two detachment bands (X' and A') at 193 nm. From [67].

feature of $NaK(SO_4)_2^{2-}$ was absent in the 266 nm spectrum owing to the RCB, which unequivocally confirmed the dianionic nature of the species being photodetached. Thus, the PES spectra of each anion exhibit two detachment features: X' (~1.5 eV) and A' (~3.5 eV) for the dimer dianions, X (~3.7 eV) and A (~5.7 eV) for the monomers. The separations between the two features in the dimer and monomer are the same. These features correspond to detachment from the top two occupied molecular orbitals of the T_d SO_4^{2-} group [64] perturbed by the cations, indicating the existence of largely intact SO_4^{2-} in these ion-pair species. The electron binding energies of the dimer dianions are lower than those of the monomers owing to the intramolecular Coulomb repulsion in the dianions.

Theoretical calculations of these ion pairs were further carried out by Wang *et al.* [67]. The lowest-energy geometry of $NaSO_4^-$ at the B3LYP/TZVP+ level of theory has C_{3v} symmetry, with Na coordinated to three oxygens (figure 8(*a*)). In this geometry the three S–O bonds to the three oxygens coordinated to sodium are 0.06 Å longer than the other S–O bond. The three oxygens coordinated to sodium also have the most negative charge. The lowest-energy geometry of KSO_4^- at the B3LYP/TZVP+ level of theory also has C_{3v} symmetry, similar to that of $NaSO_4^-$ (figure 8(*b*)). As expected, the K–O distances are longer than the

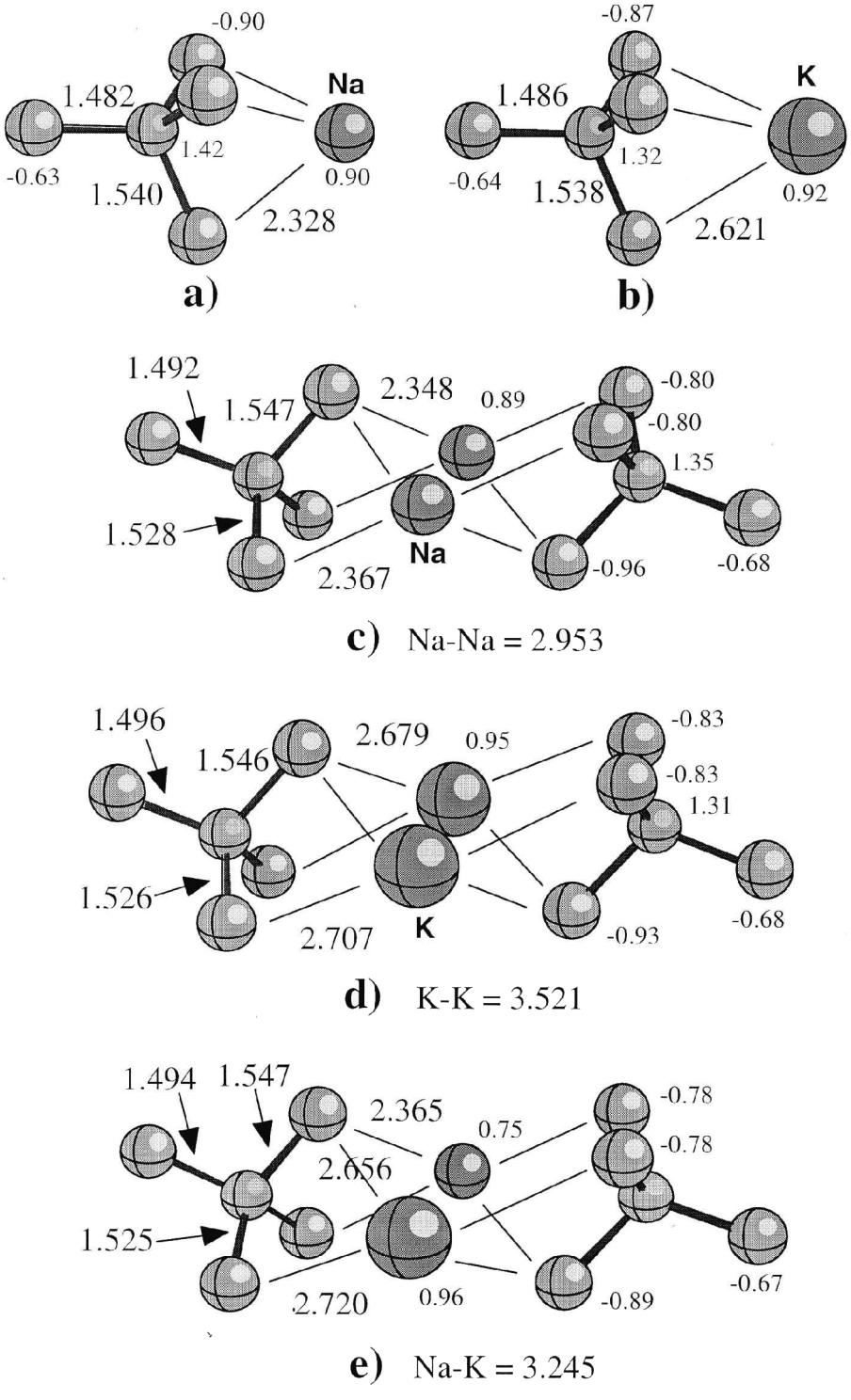

Figure 8. Optimized geometries at B3LYP/TZVP+ level for (*a*) $NaSO_4^-$, (*b*) KSO_4^-, (*c*) $(NaSO_4)_2^{2-}$, (*d*) $(KSO_4)_2^{2-}$ and (*e*) $[NaK(SO_4)_2]^{2-}$. Selected bond lengths (bold, in Å) and Mulliken partial charges ($|e|$), are indicated. From [67].

corresponding Na–O distances, consistent with the larger ionic radius of K^+. The partial charges are also very similar to those calculated for the sodium complexes.

The B3LYP/TZVP+ optimized geometry of $(NaSO_4)_2^{2-}$ is shown in figure 8(*c*). The geometry of the C_{2h} dimer dianion resembles that of the C_{3v} monomer. Three of the oxygens of each SO_4^{2-} are coordinated to Na^+. The distances between oxygen and sodium are 0.02–0.04 Å longer than in the C_{3v} monomer. The S–O bond lengths differ by about 0.01 Å. The partial charges are also similar to those of the C_{3v} monomer. The charge on sodium is essentially unchanged. The three oxygens coordinated with sodium have the greater negative charge. Apparently the Coulomb repulsion between the sodiums is overcome by the Coulomb attraction between Na^+ and SO_4^{2-} in the dimer. Figures 8(*d*) and (*e*) show the B3LYP/TZVP+ optimized geometry of $(KSO_4)_2^{2-}$ and the mixed dimer $[NaK(SO_4)_2]^{2-}$. As expected, they are qualitatively similar to that of the corresponding $(NaSO_4)_2^{2-}$. The symmetry of the mixed dimer is naturally lower (C_2) than that of the pure dimers. The structures of the dimer dianions clearly show that the alkali metal cations bridge the two sulphate dianions.

4.2. *Solvation effect and solvation stabilization of MCAs*

The minimum number of water molecules needed to stabilize an unstable free MCA is an important question. Investigation of solvated MCAs also provides molecular-level information to aid in understanding their properties in solutions. Our first study of solvated MCAs concerned a series of linear dicarboxylate dianions solvated by one and two water molecules, $^-O_2C–(CH_2)_n–CO_2^-(H_2O)_x$ $(x = 1, 2)$ [42]. We found that one water molecule is enough to stabilize $^-O_2C–(CH_2)_2–CO_2^-$, the succinate dianion, which is unstable as shown in section 3.3. We observed that the first water molecule stabilizes the electron binding energy by 0.3 eV, whereas the second water molecule stabilizes the binding energies by twice as much, suggesting that each water molecule solvates one carboxylate group.

We have been very interested in how SO_4^{2-} is stabilized in the gas phase by water because SO_4^{2-} is one of the most common inorganic MCAs. We were able to produce hydrated sulphate clusters for a broad size range, $SO_4^{2-}(H_2O)_n$, $n = 3$–60, and investigated them systematically using PES [68–70]. Figure 9 shows a set of typical mass spectra of $SO_4^{2-}(H_2O)_n$ clusters from our ESI source and measured using our ion-trap TOF technique [70]. The smallest cluster observed had $n = 3$. We could not detect any clusters with one or two H_2O, consistent with a previous experiment, in which the smallest cluster observed had $n = 4$ [36]. The mass spectrum indicated that SO_4^{2-} needs at least three H_2O to be stabilized.

Figure 10 shows the 157 nm PES spectra of $SO_4^{2-}(H_2O)_n$ for $n = 4$–40. In the smaller size range $(n \leqslant 12)$, the PES spectra remain similar and also similar to the spectrum of $NaSO_4^-$, suggesting that the electrons being detached are from the SO_4^{2-} solute. The adiabatic electron detachment energies of the hydrated cluster dianions were observed to increase steadily, but not linearly, with the number of water molecules, from ~0.4 for $n = 3$ [68] to ~5.7 eV for $n = 40$ [69]. From the previously calculated electron binding energy of −1.6 eV for free SO_4^{2-} [64], our measured electron binding energy of 1.0 eV for $n = 4$ implies that the first four H_2O stabilize SO_4^{2-} by ~2.6 eV, giving an average stabilization of ~0.65 eV per H_2O. The measured increase of electron binding energy from $n = 3$ to 4 is ~0.6 eV, suggesting that each of the first four water molecules has approximately the same stabilizing

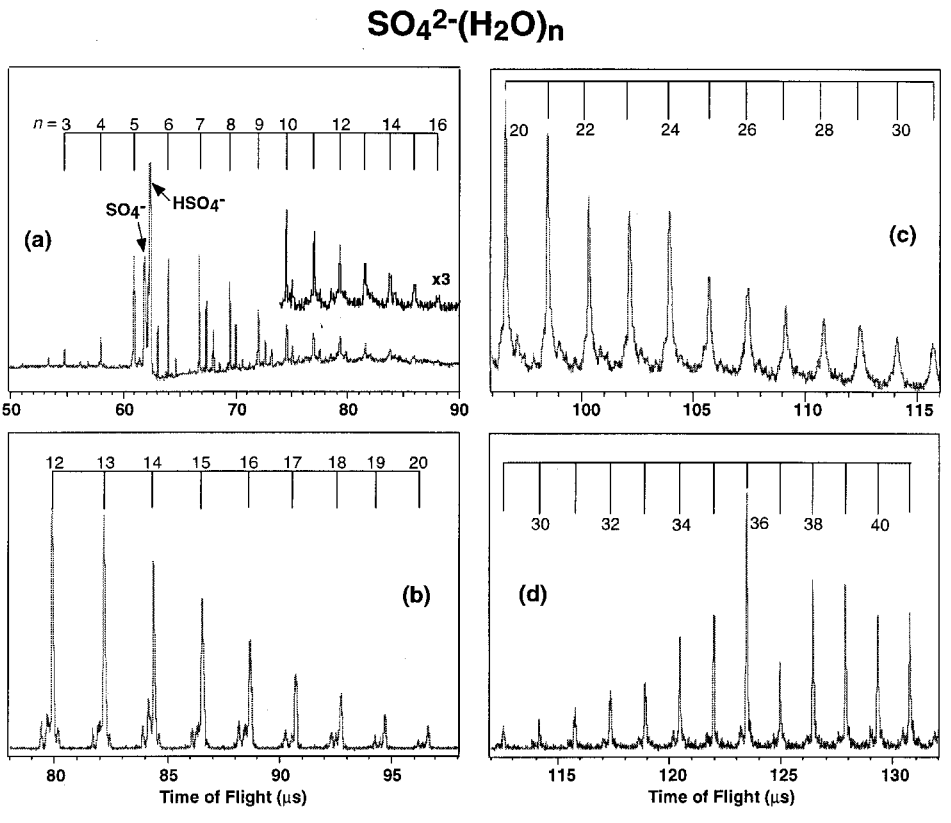

Figure 9. Typical mass spectra of $SO_4^{2-}(H_2O)_n$ using electrospray of a tetra-butyl ammonium sulphate solution and optimized for different cluster size ranges: (*a*) $n = 3$–16, (*b*) $n = 12$–20, (*c*) $n = 20$–31 and (*d*) $n = 31$–41. Note the general monotonic decrease of ion intensity as a function of size and the intense peak of $n = 36$. From [70].

effect on SO_4^{2-}. From the 0.4 eV binding energy measured currently for $SO_4^{2-}(H_2O)_3$, we extrapolate that one or two H_2O are not sufficient to stabilize SO_4^{2-}; each is still electronically unstable by roughly -0.9 and -0.2 eV respectively. The photodetachment results thus provide the most conclusive evidence that *three* is the minimum number of H_2O needed to stabilize a free SO_4^{2-}. The first four water molecules seem to have the strongest stabilizing effect. The incremental stabilization drops to ~0.4 eV for $n = 5$ and 6. For the larger clusters, the stepwise stabilization becomes even smaller, decreasing smoothly: ~0.3 eV for $n = 7$ and 8; ~0.25 eV for $n = 9$ and 10; ~0.2 eV for $n > 10$ [68].

We further performed theoretical calculations in collaboration with Nicholas to determine the minimum energy structures of $SO_4^{2-}(H_2O)_n$ (figure 11) and to obtain a more quantitative picture about how SO_4^{2-} is solvated by H_2O [68]. The theoretical results confirmed indeed that $SO_4^{2-}(H_2O)$ and $SO_4^{2-}(H_2O)_2$ are electronically unstable; the calculated adiabatic binding energies for them are -0.91 and -0.22 eV, respectively, in excellent agreement with our extrapolated values from the experimental data, as discussed above. The calculations further confirmed that SO_4^{2-} exists as a distinct structural unit with minimal perturbations in all the solvated clusters; the S–O bond lengths and angles differ only slightly from the ideal

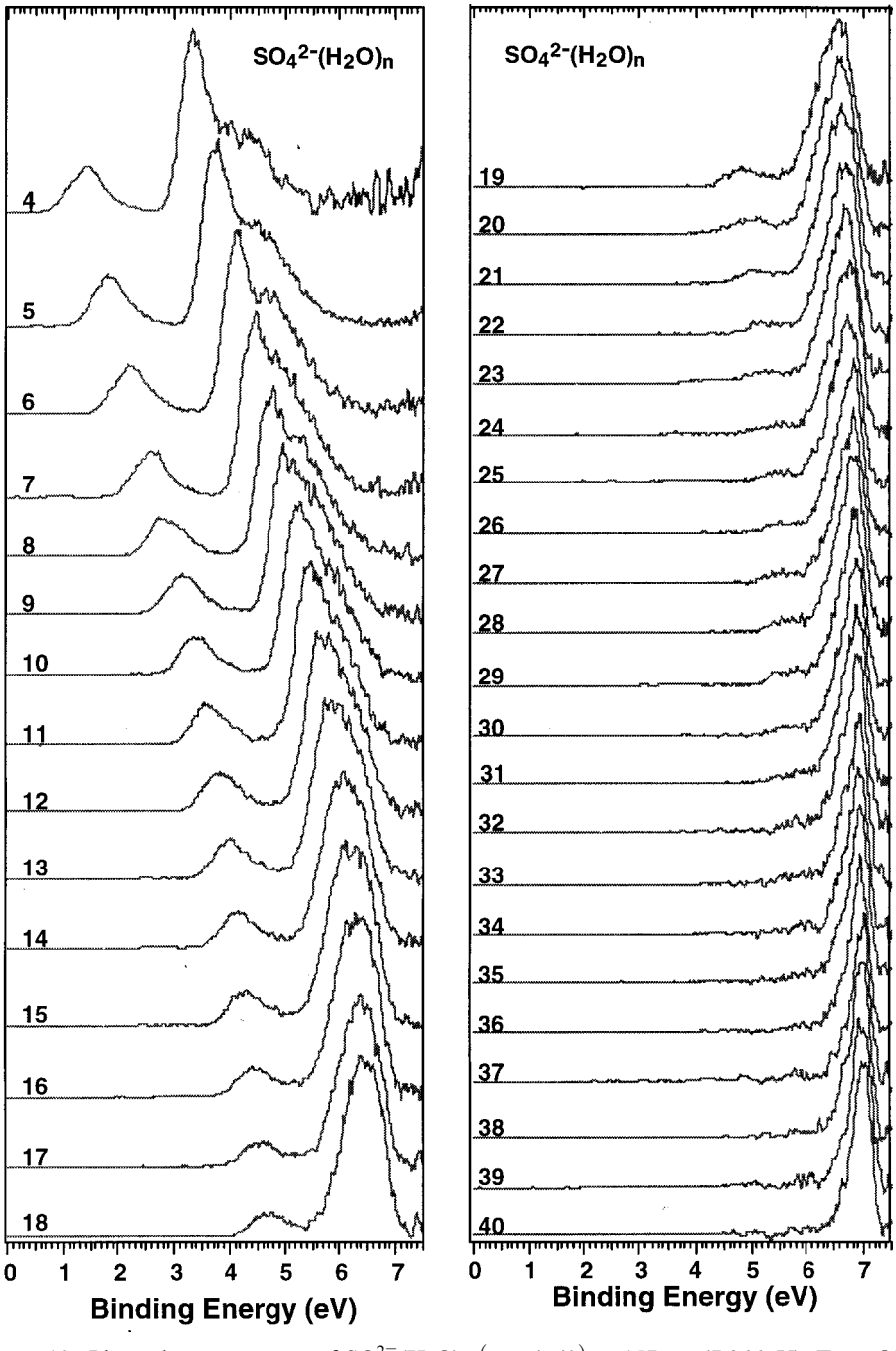

Figure 10. Photoelectron spectra of $SO_4^{2-}(H_2O)_n$ $(n = 4\text{-}40)$ at 157 nm (7.866 eV). From [69].

tetrahedral structure (calculated S–O bond lengths are 1.52 Å in isolated SO_4^{2-}) [64]. Consistent with this interpretation, there is little delocalization of charge from the SO_4^{2-} species to the surrounding water molecules; the calculated charge on SO_4 ranges from $-1.92|e|$ with one bound water molecule to $-1.90|e|$ in the complex with six waters molecules [68].

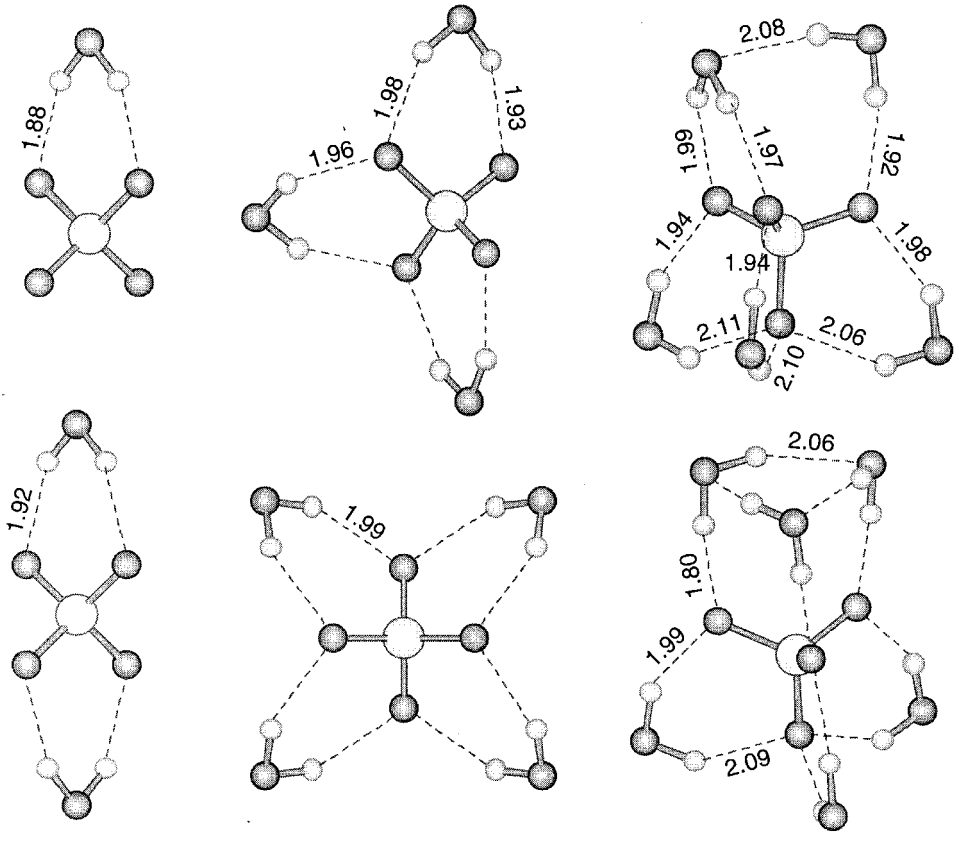

Figure 11. Optimized structures for the lowest-energy isomers of $SO_4^{2-}(H_2O)_n$ $(n = 1\text{–}6)$ at the B3LYP/TZVP+ level. The H-bond lengths (Å) are indicated. From [68].

Figure 11 shows the lowest energy optimized structures for the hydrated clusters with $n = 1$–6. A clear picture of stepwise solvation and stabilization of SO_4^{2-} emerges from the structures shown in figure 11. The first four water molecules strongly bind to SO_4^{2-}, each forming two strong H bonds around the solute. The charges of the dianion are then stabilized sufficiently that additional water molecules form only single H bonds with SO_4^{2-} and that interwater H bonding is observed starting at $n = 5$.

4.3. *Transition from gaseous hydrated clusters to aqueous solution*

As the solvent number increased above $n \approx 12$, three gradual changes were observed in the 157 nm spectra of $SO_4^{2-}(H_2O)_n$, as shown in figure 10 [69]. First, the relative intensity of the low binding energy feature from SO_4^{2-} seemed to decrease and almost disappeared in the large clusters $(n \approx 30)$. Second, a very intense peak emerged at the high binding energy side and dominated for the large clusters. Third, above $n \approx 12$, the gap between the first two bands became smaller, whereas it remained constant in the small clusters. The disappearance of the solute signals in the large $SO_4^{2-}(H_2O)_n$ clusters suggested that SO_4^{2-} is solvated in the centre of the water clusters such that photoelectrons from the centrally located solute might not readily escape the increasing solvent layers. This interpretation is supported by a

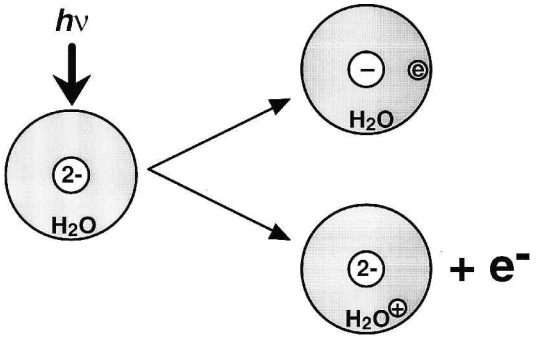

Figure 12. Schematic illustration of the photophysical processes taking place in the nano-water droplets doped with a doubly charged anion, showing the trapping of the photoelectron from the solute (top) and the ionization of the solvent (bottom). From [69].

previous PES study at 21.2 eV of a highly concentrated aqueous solution of CsF [71]. In this experiment, photoemission signals from F^- were observed to be significantly reduced by a one-layer water solvation shell on F^- at the solution–vacuum interface [72]. Our *ab initio* calculations for up to six water molecules showed that indeed the water molecules tend to solvate symmetrically around SO_4^{2-} (figure 11).

The high binding energy feature observed for the larger clusters was due to ionization of water. The ionization potential of water clusters should be between that of gaseous water molecules at 12.6 eV and that of liquid water at 10.06 eV [73]. However, because the solvated clusters were negatively charged, the ionization potentials of water in the clusters were expected to be lower. In fact, we recently observed that the ionization potential of a water molecule was reduced from 12.6 eV to about 6.1 eV in the F^-H_2O complex, because of the strong Coulomb repulsion experienced by the valence electrons in H_2O from F^- [74].

Thus we observed a smooth transition from gas-phase clusters to behaviour of electrolyte solutions as a function of cluster size in $SO_4^{2-}(H_2O)_n$. The photoelectron spectra of the small clusters of $SO_4^{2-}(H_2O)_n$ were shown to be characteristic of the solutes. However, beyond the first solvation shell $(n \approx 12)$ [75], photoemission features from the solutes were diminished and ionization of water emerged, analogous to bulk aqueous solutions. For large clusters with dimensions over 1 nm $(n \approx 30)$ the solute photoemission features almost completely disappeared and the spectra were dominated by the ionization of water. The solute photoelectrons must be trapped by the solvent, forming 'solvated' electrons in the clusters, analogous to that in bulk solutions. The two ionization processes are schematically shown in figure 12. The large solvated clusters can be used as molecular models to investigate the photophysics and chemistry of aqueous electrolyte solutions.

5. Probing the electronic structure of solution-phase species in the gas phase

5.1. *Photoelectron spectroscopy of multiply charged transition metal complexes*

Many metal complexes and redox species exist in solutions as MCAs [76]. These species have been studied extensively in the condensed phase. Gas-phase studies of these metal complexes would yield their intrinsic molecular properties without the complications of the condensed-phase environments. The obtained electronic

and spectroscopic information can be used to compare directly with theoretical calculations, which are often done for gaseous species. The apparatus that we developed is ideally suited to study these species. Our initial experimental effort was focused on the octahedral or quasi-octahedral hexahalogenometallates species, MX_6^{2-} (M = Re, Os, Ir, Pt; X = Cl, Br) [44]. These dianions are classical Werner-type transition metal complexes and are commonly found in the condensed phase [76–79]. Our photoelectron data yielded a wealth of electronic structure information about these metal complexes. By comparing the spectral features of the Cl complexes with those of the Br complexes, we were able to distinguish clearly detachment features from metal *d* orbitals or ligand orbitals. We found that detachments from the metal *d* orbitals all occur at low binding energies whereas those from the ligand-dominated orbitals all take place at higher binding energies [44].

A one-electron oxidation reaction, aside from solvation effects, is similar to electron detachment in the gas phase. Therefore, the gas-phase electron affinities should be inherently related to oxidation potentials. We indeed found a remarkable correlation between electron affinities measured *in vacuo* and the redox potentials of these species in solution [44], suggesting that the solvation energies for MX_6^{2-} are similar.

We have also obtained well-resolved PES spectra for the classical square-planar complexes $PtCl_4^{2-}$ and $PtBr_4^{2-}$ [45, 80]. The spectra for these two complexes were found to be similar, each with 10 well-resolved electronic features (figure 13). These

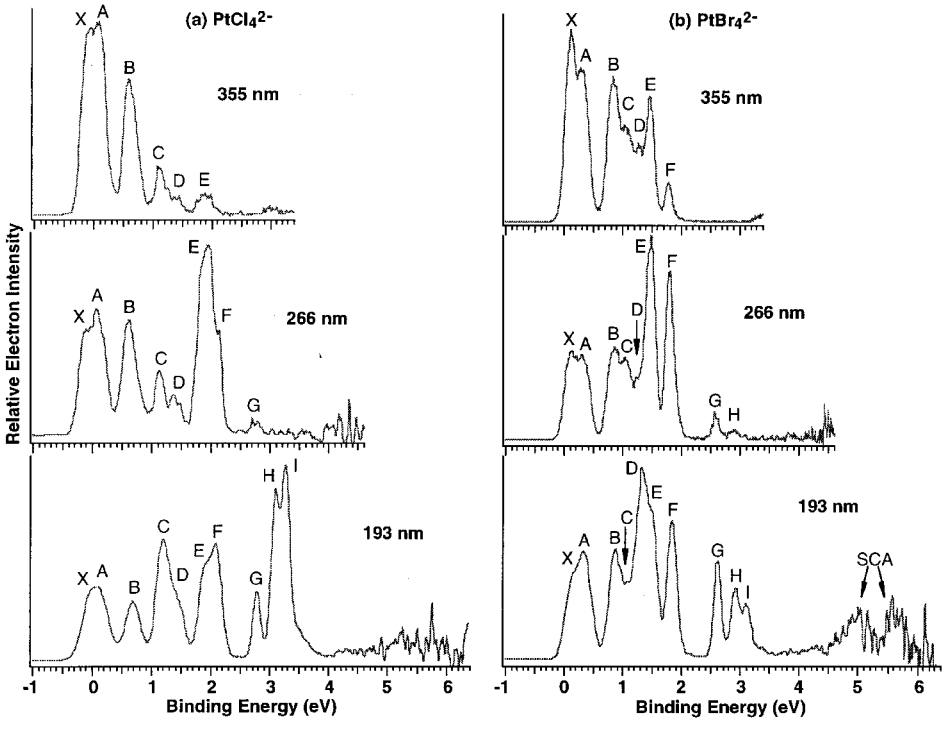

Figure 13. Photoelectron spectra of (*a*) $PtCl_4^{2-}$ and (*b*) $PtBr_4^{2-}$ at three photon energies. Note the negative binding energy features (*X*) revealed at all three different detaching photon energies. The letters label the resolved electronic features. SCA indicates a feature due to the singly charged anion. From [80].

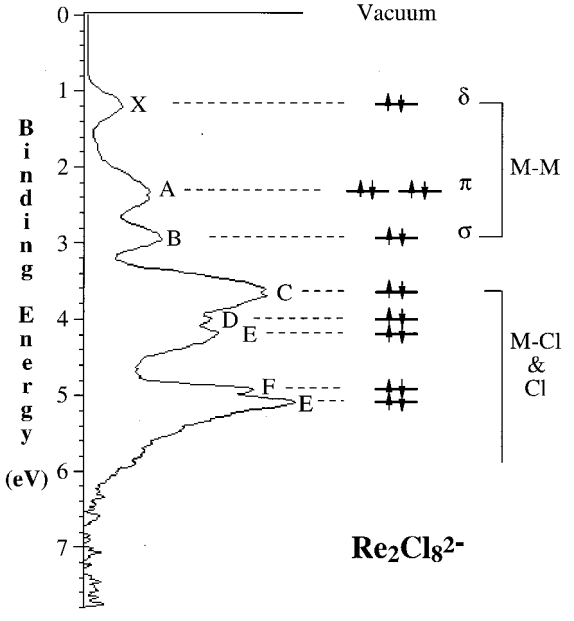

Figure 14. The 157 nm photoelectron spectrum of $Re_2Cl_8^{2-}$ with the corresponding molecular orbitals, showing the relationship between photodetachment features and the occupied molecular orbitals. From [82].

observed detachment features were qualitatively interpreted using available theoretical calculations [80]. The unprecedented resolution of the spectra afforded in the gas phase allowed us to determine definitely the ground-state molecular energy levels for these classical square-planar metal complexes. We found that in $PtCl_4^{2-}$ all the *d* orbitals are above the ligand-derived orbitals, whereas in $PtBr_4^{2-}$ all the *d* orbitals are stabilized while the ligand orbitals are destabilized, leading to an overlap between the *d* and ligand orbitals. Furthermore, the binding energies of the second excess electron in PtX_4^{2-} were found surprisingly to be *negative* by -0.25 and -0.04 eV for X = Cl and Br, respectively. The negative electron-binding energies indicate that the two gaseous dianions are in fact electronically unstable against electron loss owing to the strong intramolecular Coulomb repulsion between the two excess charges. Photon-energy-dependent studies clearly revealed the dianion nature of these species and allowed the repulsive Coulomb barriers to be estimated [80]. We also estimated the lifetimes of these two metastable dianions using the ion trap and compared with theoretical calculations using a tunnelling model, analogous to α decay [45]. More accurate lifetimes for $PtCl_4^{2-}$ and $PtBr_4^{2-}$ were obtained subsequently using ion cyclotron mass spectrometry [81].

We have also obtained well-resolved PES spectra for the classical metal complex containing a metal–metal multiple bond $[Re_2Cl_8]^{2-}$ [82]. Figure 14 shows the PES spectrum of $[Re_2Cl_8]^{2-}$ taken at 157 nm photon energy. The assignments of the PES features were also given according to the molecular orbitals [83]. The three metal–metal bonding molecular orbitals are clearly revealed at lower binding energies. These data provide unprecedented experimental electronic structure information that is valuable to verify the molecular orbital model developed for this metal complex, as well as its chemical bonding.

5.2. *Probing the electronic structure of redox species and their intrinsic reorganization energies in electron transfer reactions*

Electron transfer (ET) is among the most fundamental chemical processes and is ubiquitous in biological and chemical systems. Extensive studies of this class of reaction have led to a quantitative understanding of key factors influencing ET reaction kinetics [84–86]. The Marcus theory, developed for outer-sphere ET with weak electronic coupling, predicted the rate constant $k_{ET} = A \exp[-(\Delta G^0 + \lambda)^2/4\lambda k_B T]$, where k_B is the Boltzmann constant, A is a prefactor that includes the electronic coupling and depends on the distance between the reactants, ΔG^0 is the free energy difference between products and reactants and λ is the total reorganization energy (figure 15(*a*)). The total reorganization energy includes components due to geometry changes of the redox species or inner-sphere complexes (intramolecular or inner-sphere reorganization energy, λ_i) and due to polarization changes in the dielectric solvent medium (out-sphere or solvent reorganization energy, λ_{out}). One of the key elements in any quantitative description of ET reaction kinetics is an accurate estimate of the intrinsic reorganization energy λ_i, which is the sum of contributions from the coupled vibrations and depends on their force constants and changes in equilibrium displacements.

We have demonstrated that λ_i can be obtained for bimolecular ET reactions involving transition metal complex anions using photodetachment spectroscopy [87]. As shown in figure 15(*a*), the reorganization energy (λ) can be viewed as the total free energy of the ET products at the geometry (coordinates) of the reactants. The intramolecular reorganization energy (λ_i) is then the total potential energy of the ET products at the geometry of the reactants. For a bimolecular ET reaction involving a reductant (red) and an oxidant (oxd), λ_i would be the sum of two terms, λ_{red} and λ_{oxd}. λ_{red} is the intramolecular reorganization energy of the reductant (the potential energy of the reductant at the geometry of its oxidized form) and λ_{oxd} is the intramolecular reorganization energy of the oxidant (the potential energy of the oxidant at the geometry of its reduced form). As shown in figure 15(*b*), photodetachment is an oxidation process, which is analogous to a half-ET reaction (because there is no electron acceptor). The photoelectron spectrum reflects the Franck–Condon factors between the ground vibrational level of the Fe(II) complex and the vibrational levels of the Fe(III) complex and depends on the geometry changes between the two species. Thus, the difference between the vertical (VDE) and adiabatic (ADE) electron binding energies is equivalent to λ_{oxd}.

We have obtained PES spectra of several Fe(II) complexes (figure 16), from which λ_{oxd} can be evaluated [87]. The most striking feature in the photoelectron spectra of the Fe(II) complexes is the weak low binding energy band in each case, regardless of the ligand type or number. By comparing the spectra of the Fe(II) complexes with those of the Fe(III) complexes, we show that the low-energy band in the spectra of the Fe(II) complexes should be due to ionization of the most loosely bound 3*d* electron, which would have been transferred in a redox reaction. Thus, the difference between the ADE and VDE of this band yields λ_{oxd}. Figure 16 also shows that the electron binding energies of the Fe(II) complexes are all much lower than those of the corresponding Fe(III) complexes, consistent with the reducing capability of the Fe(II) complexes, one of the most common classes of reducing agents, particularly in biomolecules involving haem proteins and Fe–S proteins [88].

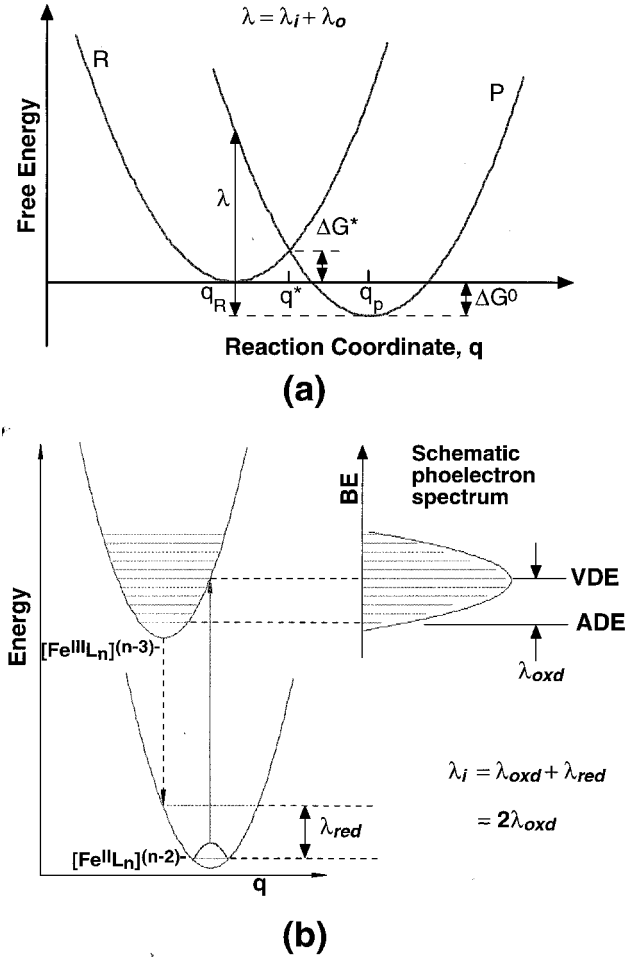

Figure 15. (*a*) The Marcus diabatic free energy curves for unsymmetrical electron transfer reactions: λ, reorganization energy (equal to the sum of the intramolecular reorganization energy, λ_i, and the outer-sphere reorganization energy, λ_o); ΔG^*, activation barrier; ΔG^0, free energy difference between reactants and products. (*b*) Schematic potential energy curves showing photodetachment of an Fe(II) complex and the hypothetical photoelectron spectrum. The difference between the vertical (VDE) and adiabatic (ADE) binding energies represents the potential energy of the Fe(III) complex at the geometry of the Fe(II) complex and is called the oxidant intramolecular reorganization energy (λ_{oxd}). For a full bimolecular ET reaction, $\lambda_i = \lambda_{oxd} + \lambda_{red}$, where λ_{red} is the reductant intramolecular reorganization energy. For self-exchange reactions $(\Delta G^0 = 0)$ and assuming that the curvature of the oxidant and reductant are similar, $\lambda_i \approx 2\lambda_{oxd}$. From [87].

6. Conclusions

We have shown in this overview some of our initial efforts to probe solution-phase species and processes in the gas phase. MCAs are an important class of solution-phase species, and our experimental method coupling electrospray and PES has made it possible for the first time to study systematically the physical properties of these species in the gas phase. The RCB, universally present in MCAs owing to the intramolecular Coulomb repulsion, has been observed directly and its effect on

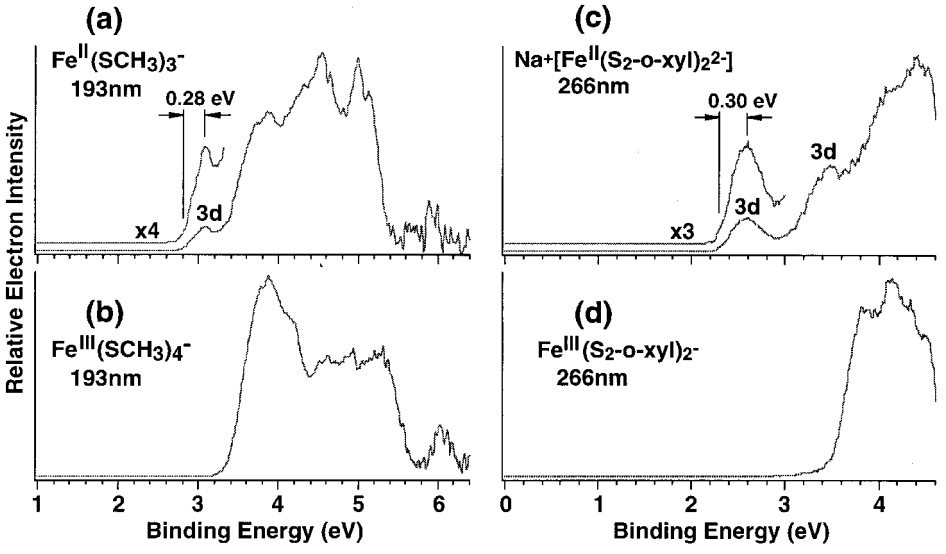

Figure 16. Photoelectron spectra of (*a*) $Fe^{II}(SCH_3)_3^-$ and (*b*) $Fe^{III}(SCH_3)_4^-$ at 193 nm and (*c*) $Na^+[Fe^{II}(S_2\text{-}o\text{-xyl})_2^{2-}]$ and (d) $Fe^{III}(S_2\text{-}o\text{-xyl})_2^-$ at 266 nm. From [87].

PES has been elucidated. Besides what have been reviewed previously in [33], we have observed that RCBs for different detachment channels of a large MCA depend on the nature of the molecular orbitals from which electrons are being detached [50]. We further showed that PES of MCAs is an ideal technique to obtain higher-order EAs. The various factors governing the stabilities of an MCA have been investigated, using two small dicarboxylate dianions with similar sizes as examples [51].

More exciting is the prospect that we now have available to us a means to investigate solution-phase chemistry in the gas phase through solvated clusters of complex anions. We have observed ion pairs and salt-bridge complexes involving SO_4^{2-} [67], which are important in understanding properties of sulphate solutions. Our studies have shown that the ion pairs and salt-bridge complexes can be viewed as intact sulphate dianions perturbed by the surrounding cations. Solvation effects and solvent stabilization of MCAs are critical issues pertinent to solution-phase chemistry and can be uniquely investigated with the ESI and PES techniques developed in our laboratory [68–70, 89]. An extensive effort was made to study the solvation and solvent stabilization of SO_4^{2-}. We found that SO_4^{2-} needs at least three water molecules to be stabilized in the gas phase. The first four water molecules strongly interact with the SO_4^{2-} core, each forming two H bonds. Water molecules were found to nucleate around the SO_4^{2-} solute owing to the strong solute–solvent interactions. Large solvated SO_4^{2-} clusters already exhibit bulk-like behaviours, can be viewed as nano-water droplets doped with an SO_4^{2-} ion and can be extrapolated to model infinitely diluted solutions [69].

The ESI–PES technique also allows a wide range of inorganic metal complexes to be investigated in the gas phase. Detailed energetics and electronic structure information about these metal complexes can be obtained because of the absence of the condensed media. One particularly interesting class of metal complexes is the redox species. We showed that PES not only allows the energetics and electronic structure of these species to be obtained but also can yield information about the

inner-shell reorganization energies in ET reactions [87]. Many other solution species can be investigated in the gas phase using ESI and PES, such intramolecular H-bonded species, organic anions and free radicals, zwitterions [90], and perhaps even DNAs and proteins. It is fair to say that the electrospray technique combined with photodetachment PES provides a unique and general tool that has the promise to probing a wide range of solution-phase phenomena and species in the gas phase with molecular details and specificity.

Acknowledgments

We thank Dr. John B. Nicholas and Professor John Simons for many interesting discussions and theoretical collaborations. The work described in this article has been supported by several sources. These include the National Science Foundation under Grant CHE-9817811, the Petroleum Research Fund administered by the American Chemical Society and the US Department of Energy (DOE), Office of Basic Energy Sciences, Chemical Science Division. The work was performed at the W. R. Wiley Environmental Molecular Sciences Laboratory, a national scientific user facility sponsored by DOE's Office of Biological and Environmental Research and located at Pacific Northwest National Laboratory, which is operated for DOE by Battelle under Contract No. DE-AC06-76RLO 1830.

References

[1] Marcus, Y., 1985, *Ion Solvation* (New York: Wiley).
[2] Pasquarello, A., Petri, I., Salmon, P. S., Parisel, O., Car, R., Toth, E., Powell, D. H., Fischer, H. E., Heim, L., and Merbach, A. E., 2001, *Science*, **291**, 856.
[3] Kropman, M. F., and Bakker, H. J., 2001, *Science*, **291**, 2118.
[4] Geissler, P. L., Dellago, C., Chandler, D., Hutter, J., and Parrinello, M., 2001, *Science*, **291**, 2121.
[5] Dedonder-Lardeux, C., Grégoire, G., Jouvet, C., Martrenchard, S., and Solgadi, D., 2000, *Chem. Rev.*, **100**, 4023.
[6] Peslherbe, G. H., Ladanyi, B. M., and Hynes, J. T., 2000, *Chem. Phys.*, **258**, 201.
[7] Scoles, G., and Lehmann, K. K., 2000, *Science*, **287**, 2429.
[8] Niedner-Schatteburg, G., and Bondybey, V. E., 2000, *Chem. Rev.*, **100**, 4059.
[9] Wright, R. R., Walker, N. R., Firth, S., and Stace, A. J., 2001, *J. phys. Chem.* A, **105**, 54.
[10] Cabarcos, O. M., Weinheimer, C. J., and Lisy, J. M., 2001, *J. chem. Phys.*, **110**, 8429.
[11] Steel, E. A., Merz, K. M., Jr., Selinger, A., and Castleman, A. W., Jr., 1995, *J. phys. Chem.*, **99**, 7829.
[12] Blades, A. T., Jayaweera, P., Ikonomou, M. G., and Kebarle, P., 1990, *J. chem. Phys.*, **92**, 5900.
[13] Thompson, C. J., Husband, J., Aguirre, F., and B. Metz, R. B., 2000, *J. phys. Chem.* A, **104**, 8155.
[14] Balbuena, P. B., Johnston, K. P., and Rossky, P. J. 1996, *J. phys. Chem.*, **100**, 2705.
[15] Markovich, G., Pollack, S., Giniger, R., and Cheshnovsky, O., 1994, *J. chem. Phys.*, **101**, 9344.
[16] Ayotte, P., Weddle, G. H., and Johnson, M. A., 1999, *J. chem. Phys.*, **110**, 7129.
[17] Cabarcos, O. M., Weinheimer, C. J., Lisy, J. M., and Xantheas, S. S., 1999, *J. chem. Phys.*, **110**, 5.
[18] Choi, J. H., Kuwata, K. T., Cao, Y. B., and Okumura, M., 1998, *J. phys. Chem.* A, **102**, 503.
[19] Lehr, L., Zanni, M. T., Frischkorn, C., Weinkauf, R., and Neumark, D. M., 1999, *Science*, **284**, 635.
[20] Tobias, D. J., Jungwirth, P., and Parrinello, M., 2001, *J. chem. Phys.*, **114**, 7036.

[21] Weber, J. M., Kelley, J. A., Nielsen, S. B., Ayotte, P., and Johnson, M. A., 2000, *Science*, **287**, 2461.
[22] Yarne, D. A., Tuckerman, M. E., and Klein, M. L., 2000, *Chem. Phys.*, **258**, 163.
[23] Waterland, M. R., Stockwell, D., and Kelley, A. M., 2001, *J. chem. Phys.*, **114**, 6249.
[24] Greenblatt, B. J., Zanni, M. T., and Neumark, D. M., 1997, *Science*, **276**, 1675.
[25] Vorsa, V., Campagnola, P. J., Nandi, S., Larsson, M., and Lineberger, W. C., 1996, *J. chem. Phys.* **105**, 2298.
[26] Compton, R. N., 1996, *Multiply Charged Negative Ions* in *Negative Ions*, edited by V. Esaulov (Cambridge: Cambridge University Press).
[27] Freeman, G. R., and March, N. H., 1996, *J. phys. Chem.*, **100**, 4331.
[28] Kalcher, J., and Sax, A. F., 1994, *Chem. Rev.*, **94**, 2291.
[29] Scheller, M. K., Compton, R. N., and Cederbaum, L. S., 1995, *Science*, **270**, 1160.
[30] Boldyrev, A. I., Gutowski, M., and Simons, J., 1996, *Acc. chem. Res.*, **29**, 497.
[31] Schroder, D., and Schwarz, H., 1999, *J. phys. Chem.* A, **103**, 7385.
[32] Dreuw, A., and Cederbaum, L. S., 2002, *Chem. Rev.*, **102**, 181.
[33] Wang, L. S., and Wang, X. B., 2000, *J. phys. Chem.* A, **104**, 1978.
[34] Wang, L. S., Ding, C. F., Wang, X. B., and Barlow, S. E., 1999, *Rev. sci. Instrum.*, **70**, 1957.
[35] Fenn, J. B., Mann, M., Meng, C. K., Wong, S. F., and Whitehouse, C. M., 1989, *Science*, **246**, 64.
[36] Blades, A. T., and Kebarle, P., 1994, *J. Am. Chem. Soc.*, **116**, 10761.
[37] Blades, A. T., Klassen, J. S., and Kebarle, P., 1995, *J. Am. Chem. Soc.*, **117**, 10563.
[38] Blades, A. T., Ho, Y., and Kebarle, P., 1996, *J. phys. Chem.*, **100**, 2443.
[39] Lau, T. C., Wang, J., Guevremont, R., and Siu, K. W. M., 1995, *J. chem. Soc., Chem. Commun.*, 877.
[40] Wang, X. B., Ding, C. F., and Wang, L. S., 1998, *Phys. Rev. Lett.*, **81**, 3351.
[41] Wang, L. S., Ding, C. F., Wang, X. B., and Nicholas, J. B., 1998, *Phys. Rev. Lett.*, **81**, 2667.
[42] Ding, C. F., Wang, X. B., and Wang, L. S., 1998, *J. phys. Chem.* A, **102**, 8633.
[43] Ding, C. F., Wang, X. B., and Wang, L. S., 1999, *J. chem. Phys.*, **110**, 3635.
[44] Wang, X. B., and Wang, L. S., 1999, *J. chem. Phys.*, **111**, 4497.
[45] Wang, X. B., and Wang, L. S., 1999, *Phys. Rev. Lett.*, **83**, 3402.
[46] Wang, X. B., and Wang, L. S., 1999, *Nature*, **400**, 245.
[47] Wang, X. B., Ferris, K., and Wang, L. S., 2000, *J. phys. Chem.* A, **104**, 1978.
[48] Wang, X. B., Ding, C. F., and Wang, L. S., 1999, *Chem. Phys. Lett.*, **307**, 391.
[49] Dreuw, A., and Cederbaum, L. S., 2000, *J. chem. Phys.*, **112**, 7400.
[50] Wang, X. B., Nicholas, J. B., and Wang, L. S., 2000, *J. chem. Phys.*, **113**, 653.
[51] Skurski, P., Simons, J., Wang, X. B., and Wang, L. S., 2000, *J. Am. Chem. Soc.*, **122**, 4499.
[52] Rienstra-Kiracofe, J. C., Tschumper, G. S., Schaefer, H. F., Nandi, S., and Ellison, G. B., 2002, *Chem. Rev.*, **102**, 231.
[53] Miyoshi, E., and Sakai, Y., 1988, *J. chem. Phys.*, **89**, 7363.
[54] Gutsev, G. L., and Boldyrev, A. I., 1990, *J. phys. Chem.*, **94**, 2256.
[55] Ewig, C. S., and Van Wazer, J. R., 1990, *J. Am. Chem. Soc.*, **112**, 109.
[56] Gutsev, G. L., 1991, *Chem. Phys. Lett.*, **184**, 305.
[57] Korobov, M. V., Kuznetsov, S. V., Sidorov, L. N., Shipachev, V. A., and Mit'kin, V. N., 1989, *Int. J. Mass Spectrom. Ion Phys.*, **87**, 13.
[58] Gutowski, M., Boldyrev, A. I., Ortiz, J. V., and Simons, J., 1994, *J. Am. Chem. Soc.*, **116**, 9262.
[59] Gutowski, M., Boldyrev, A. I., Simons, J., Rak, J., and Blazejowski, J., 1996, *J. Am. Chem. Soc.*, **118**, 1173.
[60] Wang, X. B., and Wang, L. S., 2000, *J. phys. Chem.* A, **104**, 4429.
[61] Stefanovich, E. V., Boldyrev, A. I., Truong, T. N., and Simons, J., 1998, *J. phys. Chem.* B., **102**, 4205.
[62] Vandenbosch, R., Will, D. I., Cooper, C., Henry, B., and Liang, J. F., 1997, *Chem. Phys. Lett.*, **274**, 112.
[63] Dreuw, A., and Cederbaum, L. S., 1999, *J. chem. Phys.*, **111**, 1467.

[64] BOLDYREV, A. I., and SIMONS, J., 1994, *J. phys. Chem.*, **98**, 2298.
[65] SIMONS, J., SKURSKI, P., and BARRIOS, R., 2000, *J. Am. Soc. Soc.*, **122**, 11893.
[66] WHITEHEAD, A., BARRIOS, R., and SIMONS, J., 2002, *J. chem. Phys.*, **116**, 2848.
[67] WANG, X. B., DING, C. F., NICHOLAS, J. B., DIXON, D. A., and WANG, L. S., 1999, *J. phys. Chem.* A, **103**, 3423.
[68] WANG, X. B., NICHOLAS, J. B., and WANG, L. S., 2000, *J. chem. Phys.*, **113**, 10837.
[69] WANG, X. B., YANG, X., NICHOLAS, J. B., and WANG, L. S., 2001, *Science*, **294**, 1322.
[70] YANG, X., WANG, X. B., and WANG, L. S., 2002, *J. phys. Chem.* B, **106**, XXX.
[71] BOHM, R., MORGNER, H., OBERBRODHAGE, J., and WULF, M., 1994, *Surf. Sci.*, **317**, 407.
[72] DIETTER, J., and MORGNER, H., 1997, *Chem. Phys.*, **220**, 261.
[73] DELAHAY, P., 1982, *Acc. chem. Res.*, **15**, 40.
[74] YANG, X., WANG, X. B., and WANG, L. S., 2001, *J. chem. Phys.*, **115**, 2889.
[75] CANNON, W. R., PETTITT, B. M., and MCCAMMON, J. A., 1994, *J. phys. Chem.*, **98**, 6225.
[76] COTTON, F. A., and WILKINSON, G., 1988, *Advanced Inorganic Chemistry* (New York: Wiley).
[77] BRAY, M. R., DEETH, R. J., PAGET, V. J., and SHEEN, P. D., 1996, *Int. J. Quan. Chem.*, **61**, 85.
[78] MACGREGOR, S. A., and MOOCK, K. H., 1998, *Inorg. Chem.*, **37**, 3284.
[79] KIM, E. E., ERIKS, K., and MAGNUSON, R., 1984, *Inorg. Chem.*, **23**, 393.
[80] WANG, X. B., and WANG, L. S., 2000, *J. Am. Chem. Soc.*, **122**, 2339.
[81] WEIS, P., HAMPE, O., GILB, S., and KAPPES, M. M., 2000, *Chem. Phys. Lett.*, **321**, 426.
[82] WANG, X. B., and WANG, L. S., 2000, *J. Am. Chem. Soc.*, **122**, 2096.
[83] COTTON, F. A., 1980, *J. mol. Struct.*, **59**, 97.
[84] MARCUS, R. A., 1993, *Rev. mod. Phys.*, **65**, 599.
[85] MARCUS, R. A., and SUTIN, N., 1985, *Biochim. Biophys. Acta*, **811**, 265.
[86] BARBARA, P. F., MEYER, T. J., and RATNER, M. A., 1996, *J. phys. Chem.*, **100**, 13148.
[87] WANG, X. B., and WANG, L. S., 2000, *J. chem. Phys.*, **112**, 6959.
[88] BEINERT, H., HOLM, R. H., and MUNCK, E., 1997, *Science*, **277**, 653.
[89] WANG, X. B., YANG, X., WANG, L. S., and NICHOLAS, J. B., 2002, *J. chem. Phys.*, **116**, 561.
[90] WANG, X. B., BROADUS, K. M., WANG, L. S., and KASS, S., 2000, *J. Am. Chem. Soc.*, **122**, 8305.